Available online at www.sciencedirect.com
ScienceDirect
International Journal of Solids and Structures 45 (2008) 676–687
INTERNATIONAL JOURNAL OF SOLIDS AND STRUCTURES
www.elsevier.com/locate/ijsolstr

Non-slipping JKR model for transversely isotropic materials

S. Chen [a,*], C. Yan [a], A. Soh [b]

[a] LNM, Institute of Mechanics, Chinese Academy of Sciences, Beijing 100080, China
[b] Department of Mechanical Engineering, The University of Hong Kong, Hong Kong, China

Received 2 March 2007; received in revised form 7 July 2007
Available online 6 September 2007

Abstract

A generalized plane strain JKR model is established for non-slipping adhesive contact between an elastic transversely isotropic cylinder and a dissimilar elastic transversely isotropic half plane, in which a pulling force acts on the cylinder with the pulling direction at an angle inclined to the contact interface. Full-coupled solutions are obtained through the Griffith energy balance between elastic and surface energies. The analysis shows that, for a special case, i.e., the direction of pulling normal to the contact interface, the full-coupled solution can be approximated by a non-oscillatory one, in which the critical pull-off force, pull-off contact half-width and adhesion strength can be expressed explicitly. For the other cases, i.e., the direction of pulling inclined to the contact interface, tangential tractions have significant effects on the pull-off process, it should be described by an exact full-coupled solution. The elastic anisotropy leads to an orientation-dependent pull-off force and adhesion strength. This study could not only supply an exact solution to the generalized JKR model of transversely isotropic materials, but also suggest a reversible adhesion sensor designed by transversely isotropic materials, such as PZT or fiber-reinforced materials with parallel fibers.

Keywords: Adhesion; Adhesive contact; Transversely isotropic material; JKR model

1. Introduction

The mechanics of contact between solid hemispheres has been used extensively in studying the surface energy of materials during the past decade (for examples, Barquins, 1988; Carpick et al., 1996; Baney and Hui, 1997; Greenwood, 1997; Johnson and Greenwood, 1997; Barthel, 1998; Greenwood and Johnson, 1998; Kim et al., 1998; Robbe-Valloire and Barquins, 1998; Morrow et al., 2003; Schwarz, 2003). Four main theories have been developed to describe the history of this contact problem: those of Hertz (1882), Johnson et al. (1971), Derjaguin et al. (1975), and Maugis (1992). While the Hertz theory (Hertz, 1882) assumes that adhesion between the spheres cannot be sustained, the JKR, DMT and MD theories do allow for adhesion by taking into account the surface energies of the bodies. In the JKR (Johnson et al., 1971) model, an equilibrium contact area is established via Griffith energy balance between elastic energy and surface energy, which results

* Corresponding author. Tel.: +86 10 82543960; fax: +86 10 82543977.
E-mail address: chenshaohua72@hotmail.com (S. Chen).

0020-7683/$ - see front matter © 2007 Elsevier Ltd. All rights reserved.
doi:10.1016/j.ijsolstr.2007.08.013

in compressive stress in the central region of contact and crack-like singular tensile stress near the edge of contact; the contact area remains finite until a critical pull-off force is reached. In the DMT model (Derjaguin et al., 1975), molecular forces outside the Hertz contact area are considered, but these forces are assumed not to change the contact profile of the Hertz solution and the tensile stress is finite in the cohesive zone outside the contact area but zero inside it. This paradox was solved by Maugis (1992), who developed a unified model linking the JKR and DMT models by extending the Dugdale model (Dugdale, 1960) of a plastic crack to the case of adhesive contact between two elastic spheres.

Most of the existing models on contact mechanics are related to isotropic materials and the tangential tractions in the contact region are neglected or regarded as frictional one to uncouple the normal and tangential stresses (Johnson, 1985). For a nanometer-sized contact, most of the phenomena will be different from those predicted by JKR theory which is not the only description of bodies in adhesive contact but is rather the limiting case of a continuous regime of contact mechanics. For example, Carpick et al. (1996) did nanometer-sized contact experiment and found that the tip-sample adhesion and the measured frictional forces unexpectedly decreased by more than one order of magnitude when scanning the tip in contact with the mica sample. They attribute the friction and adhesion decreases to changes of the interface, either structure or chemical, as opposed to changes in bulk structure or properties. Although several features unique to the nanoscale were observed in the experiment study of adhesion and friction for nano-asperities (Enachescu et al., 1999; Carpick et al., 2004), they found that the friction is proportional to the true contact area, the interfacial shear strength and the work of adhesion can be determined in the framework of fracture mechanics. The near-ideal shear strength observed in the experiment can be explained using dislocation models (Hurtado and Kim, 1999). For macroscopic contact, Kendall (1975) investigated the effects of shrinkage stress on a \brittle interfacial failure of a bonded laminate. Savkoor and Briggs (1977) showed that an applied tangential force can reduce the area of contact between elastic solids.

With the developing of bio-mechanics and bionics, contact mechanics has been used to understand biological adhesion mechanism (Arzt et al., 2003; Geim et al., 2003; Persson, 2003; Glassmaker et al., 2004; Gao and Yao, 2004; Hui et al., 2004; Chu et al., 2005; Gao et al., 2005). In some cases, perfect bonding should be considered because the effects of tangential traction on the pull-off process cannot be neglected (Chen and Gao, 2006a,b,c, 2007). Recent studies on elastic bodies in non-slipping adhesive contact with a laterally stretched substrate (Chen and Gao, 2006a,b) indicate that the substrate strain can have significant effect on the contact area. The pull-off process of two elastic spheres in non-slipping adhesive contact under a pair of pulling forces and a mismatch strain will be influenced by the mismatch strain significantly (Chen and Gao, 2006c). Furthermore, isotropy is not enough sometimes to describe the material characters (Gao et al., 2005; Yao and Gao, 2006; Chen and Gao, 2007), such as the attachment pad of grasshopper and cicada (Slifer, 1950; Roth and Willis, 1952; Arnold, 1974), the tissue of gecko's feet (Autumn et al., 2000).

As an extension of the adhesive contact model for isotropic materials (Chen and Wang, 2006), in the present paper, a generalized adhesive contact model between two dissimilar transversely isotropic solids is investigated. The contact region is also assumed to be perfect bonding, then, an external loading is added obliquely on the cylinder. Exact solutions to the generalized JKR model for transversely isotropic materials will be given and analyzed. The results suggest that an orientation-dependent adhesion sensor could be designed by transversely isotropic materials, such as PZT-4 and fiber-reinforced composites, where all fibers are in parallel. Furthermore, explicit solutions can be deduced from the generalized model for some special and useful cases, such as adhesive contact between a rigid cylinder and a transversely isotropic half plane or between an isotropic solid and a transversely isotropic substrate, only if the direction of pulling force is normal to the contact interface.

2. Elastic constants and Barnett–Lothe tensors for transversely isotropic material

A special class of orthotropic materials are those that have the same properties in one plane (e.g., the $x - z$ plane) and different properties in the direction normal to this plane (e.g., the y-axis). Such materials are called transversely isotropic, and they are described by five independent elastic constants, instead of nine for fully orthotropic.

Examples of transversely isotropic materials include some piezoelectric materials (e.g., PZT-4, barium titanate) and fiber-reinforced composites where all fibers are in parallel.

By convention, the five elastic constants in transverse isotropic constitutive equations are the Young's modulus and Poisson ratio in the $x-z$ symmetry plane, E_1 and v_1, the Young's modulus and Poisson ratio in the y-direction, E_2 and v_2, and the shear modulus in the y-direction G_{12}.

For orthotropic materials, Dongye and Ting (1989) and Hwu (1993) have shown the explicit expressions for the Barnett–Lothe tensors $\boldsymbol{S}$ and $\boldsymbol{L}$, which are real matrices composed of the elasticity constants. For plane strain transversely isotropic materials, the corresponding Barnett–Lothe tensors $\boldsymbol{S}$ and $\boldsymbol{L}$ can be reduced as

$$\boldsymbol{S}=\begin{bmatrix}0 & s_{12}\\ s_{21} & 0\end{bmatrix},\quad \boldsymbol{L}=\begin{bmatrix}L_{11} & 0\\ 0 & L_{22}\end{bmatrix}, \tag{1}$$

where

$$s_{12}=-\alpha_2\gamma_1\chi_1,\quad s_{21}=\alpha_1\gamma_2\chi_1, \tag{2}$$

$$L_{11}=\alpha_1\gamma_1E_1,\quad L_{22}=\alpha_2\gamma_2E_2, \tag{3}$$

$$\begin{cases}\gamma_1=\left(E_1/G_{12}+2\chi_1\sqrt{E_1/E_2}\right)^{-1/2}, & \gamma_2=\left(E_2/G_{12}+2\chi_1\sqrt{E_2/E_1}\right)^{-1/2},\\ \alpha_1=\left(1-v_1^2\right)^{-1/2}, & \alpha_2=\left(1-\frac{v_2^2E_1}{E_2}\right)^{-1/2},\\ \chi_1=\sqrt{(1-v_1^2)\left(1-\frac{v_2^2E_1}{E_2}\right)}-(1+v_1)v_2\sqrt{\frac{E_1}{E_2}}, & \end{cases} \tag{4}$$

$\boldsymbol{S}$ and $\boldsymbol{L}$ tensors are often used to express the influence of material properties. In the present paper, they will be used as coefficients in the following Green equations (7).

3. Adhesive contact model for two dissimilar transversely isotropic solids

In this paper, a plane strain model as shown in Fig. 1 is investigated, in which an elastic cylinder is in adhesive contact with an elastic half plane. Both solids are transversely isotropic materials. The upper material

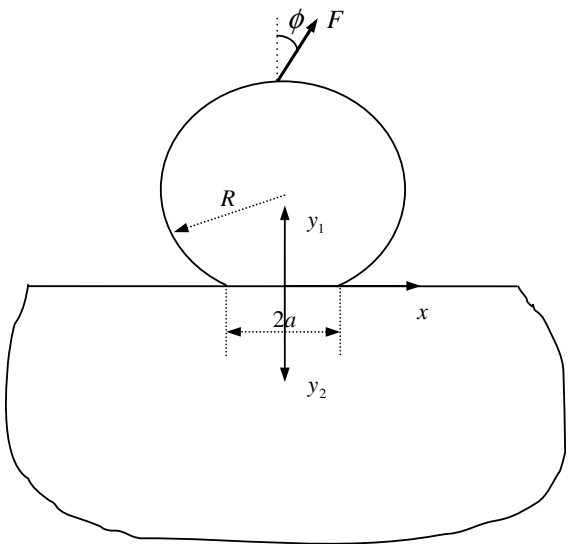

Fig. 1. The adhesive contact model between an elastic transversely isotropic cylinder of radius R and an elastic transversely isotropic half plane with contact width $2a$. Two kinds of coordinate systems (x, y_1) and (x, y_2) are fixed on the cylinder and the half plane, respectively, with the origins at the center of the contact interface.

denotes as material "1" and the lower one is material "2". R is the radius of the upper cylinder and $2a$ is the contact width. After adhesive contact, an external loading F in $x-y$ plane acts on the cylinder with an angle ϕ inclined to the normal of the contact interface as shown in Fig. 1.

Two Cartesian reference coordinate systems (x, y_1) and (x, y_2) lie at the center of the contact region with y_1 and y_2 pointing into the upper cylinder and the lower half-space, respectively. The contact region is assumed to be perfect bonding, so that the edges of the contact region resemble two opposing interfacial cracks under plane strain deformation.

As in almost all contact mechanics theories (Johnson, 1985), the contact width is assumed to be small compared to the radius of the cylinder such that the deformation of the cylinder can be approximated by that of an elastic half-space. The pulling force is assumed to be properly added such that no net bending moment on the contact region is produced.

Under the above assumptions, the continuity condition of displacements across the contact interface can be expressed as

$$\begin{cases} \bar{u}_{x1} - \bar{u}_{x2} = 0 \\ \bar{u}_{y1} + \bar{u}_{y2} = \delta - \frac{x^2}{2R} \end{cases} \quad |x| \leqslant a, \tag{5}$$

where $\bar{u}_{xj}$ $(\bar{u}_{yj})$ denotes the displacement in the x $(y_i,\ i = 1,2)$ direction of each material j $(j = 1,2)$ along the interface, δ is a constant and R the radius of the cylinder (Johnson, 1985).

The displacement gradients with respect to x yields

$$\begin{cases} \frac{\partial \bar{u}_{x1}}{\partial x} - \frac{\partial \bar{u}_{x2}}{\partial x} = 0, \\ \frac{\partial \bar{u}_{y1}}{\partial x} + \frac{\partial \bar{u}_{y2}}{\partial x} = -\frac{x}{R}. \end{cases} \tag{6}$$

Using the Green's functions of an elastic transversely isotropic half-space subjected to surface tractions (Ting, 1996) yields

$$\begin{cases} \frac{D_{11}}{\pi} \int_{-a}^{a} \frac{Q(s)}{s-x} \mathrm{d}s + W_{12} P(x) = 0, \\ \frac{D_{22}}{\pi} \int_{-a}^{a} \frac{P(s)}{s-x} \mathrm{d}s + W_{21} Q(x) = -\frac{x}{R}, \end{cases} \tag{7}$$

where $P(x)$ and $Q(x)$ denote the normal and tangential tractions along the contact interface of the cylinder, respectively. The coefficients are expressed as

$$D_{11} = \left(\frac{1}{L_{11}}\right)_1 + \left(\frac{1}{L_{11}}\right)_2, \quad D_{22} = \left(\frac{1}{L_{22}}\right)_1 + \left(\frac{1}{L_{22}}\right)_2 \tag{8}$$

and

$$W_{12} = \left(\frac{s_{12}}{L_{22}}\right)_1 - \left(\frac{s_{12}}{L_{22}}\right)_2, \quad W_{21} = \left(\frac{s_{21}}{L_{11}}\right)_1 - \left(\frac{s_{21}}{L_{11}}\right)_2, \tag{9}$$

$$W_{21} = -W_{12}, \tag{10}$$

$()_j$ denotes the term of jth $(j = 1,2)$ material.

Eq. (7) can be rewritten in a matrix form as

$$\frac{1}{\pi} \int_{-a}^{a} \frac{\boldsymbol{A}}{s-x} \boldsymbol{f}(s) \mathrm{d}s + \boldsymbol{B}\boldsymbol{f}(x) = \boldsymbol{C}, \tag{11}$$

where

$$\boldsymbol{A} = \begin{bmatrix} 1 & 0 \\ 0 & 1 \end{bmatrix}, \quad \boldsymbol{B} = \begin{bmatrix} 0 & -\frac{W_{21}}{D_{11}} \\ \frac{W_{21}}{D_{22}} & 0 \end{bmatrix}, \quad \boldsymbol{C} = \begin{bmatrix} 0 \\ \frac{-x}{D_{22}R} \end{bmatrix}, \quad \boldsymbol{f}(x) = \begin{pmatrix} Q(x) \\ P(x) \end{pmatrix}. \tag{12}$$

The calculations are quite lengthy but the methodology of solving such integral Eq. (11) is standard, which can be found in Chen and Gao (2006a), so that we skip the details and only give a brief introduction as follows.

Introducing the following transformation

$$F_k(z) = \frac{1}{2\pi \mathrm{i}} \int_{-a}^{a} \frac{f_k(s)}{s-z} \mathrm{d}s \quad k = 1, 2, \tag{13}$$

where $z = x + \mathrm{i}y$ and here $\mathrm{i} = \sqrt{-1}$, Eq. (11) can be decoupled into two inhomogeneous Hilbert equations. Following the standard procedure (Carrier et al., 1983; Chen and Gao, 2006a) to solve Hilbert equation, we can obtain the interfacial tractions $Q(x)$ and $P(x)$,

$$\begin{cases} Q(x) = 2\mathrm{Re}\{I(x)\} + \frac{x\eta}{R\sqrt{D_{11}D_{22}}(1-\eta^2)} - \frac{2\kappa_1(a+x)^{-\bar{r}}(a-x)^{-r}\mathrm{i}}{\sqrt{1-\eta^2}} - \frac{2\kappa_2(a+x)^{-r}(a-x)^{-\bar{r}}\mathrm{i}}{\sqrt{1-\eta^2}}, \\ P(x) = \left[-2\mathrm{Im}\{I(x)\} + \frac{2\kappa_1(a+x)^{-\bar{r}}(a-x)^{-r}}{\sqrt{1-\eta^2}} - \frac{2\kappa_2(a+x)^{-r}(a-x)^{-\bar{r}}}{\sqrt{1-\eta^2}}\right]\sqrt{\frac{D_{11}}{D_{22}}}, \end{cases} \tag{14}$$

where

$$I(x) = \frac{(a+x)^{-\bar{r}}(a-x)^{-r}}{2\pi \mathrm{i} R\sqrt{D_{11}D_{22}}(1-\eta^2)} \int_{-a}^{a} \frac{t(a+t)^{\bar{r}}(a-t)^{r}}{t-x} \mathrm{d}t. \tag{15}$$

The stress singularity is

$$r = \frac{1}{2} + \mathrm{i}\varepsilon, \quad \varepsilon = \frac{1}{2\pi} \ln \frac{1+\eta}{1-\eta} \tag{16}$$

and

$$\eta = |W_{21}(D_{11}D_{22})^{-1/2}| \tag{17}$$

denotes a bimaterial constant, which is analogous to Dundurs' parameters β for isotropic materials.

Using the following equilibrium conditions

$$\int_{-a}^{a} P(x)\mathrm{d}x = -F\cos\phi, \quad \int_{-a}^{a} Q(x)\mathrm{d}x = F\sin\phi \tag{18}$$

yields

$$\kappa_1 = \frac{-\sqrt{1-\eta^2}\left(F\sin\phi + \mathrm{i}F\cos\phi\sqrt{D_{22}/D_{11}}\right)}{4\mathrm{i}\int_{-a}^{a}(a+x)^{-\bar{r}}(a-x)^{-r}\mathrm{d}x}, \tag{19}$$

$$\kappa_2 = \frac{-\sqrt{1-\eta^2}\left(F\sin\phi - \mathrm{i}F\cos\phi\sqrt{D_{22}/D_{11}}\right)}{4\mathrm{i}\int_{-a}^{a}(a+x)^{-r}(a-x)^{-\bar{r}}\mathrm{d}x}. \tag{20}$$

Substituting Eqs. (19) and (20) into Eqs. (14), the interfacial tractions can be rewritten as

$$\begin{cases} Q(x) = 2\mathrm{Re}\{I(x)\} + \frac{x\eta}{R\sqrt{D_{11}D_{22}}(1-\eta^2)} + \frac{4\mathrm{Im}\left\{\kappa_1(a+x)^{-\bar{r}}(a-x)^{-r}\right\}}{\sqrt{1-\eta^2}}, \\ P(x) = \left[-2\mathrm{Im}\{I(x)\} + \frac{4\mathrm{Re}\left\{\kappa_1(a+x)^{-\bar{r}}(a-x)^{-r}\right\}}{\sqrt{1-\eta^2}}\right]\sqrt{\frac{D_{11}}{D_{22}}}. \end{cases} \tag{21}$$

According to Wu (1990), Hwu (1993) and Ting (1996), the stress intensity factors for an interface crack can be given by

$$\boldsymbol{K} = \lim_{x\to a}\sqrt{2\pi(a-x)}\boldsymbol{\Lambda}\left\langle\left\langle\left(\frac{a-x}{l}\right)^{\mathrm{i}\varepsilon_\alpha}\right\rangle\right\rangle\boldsymbol{\Lambda}^{-1}\boldsymbol{\varphi} = \begin{Bmatrix} K_{II} \\ -K_I \end{Bmatrix}, \tag{22}$$

where

$$\varepsilon_1 = \varepsilon, \quad \varepsilon_2 = -\varepsilon \tag{23}$$

and

$$\boldsymbol{\Lambda} = \begin{bmatrix} \frac{-\mathrm{i}}{\sqrt{2D_{11}}} & \frac{\mathrm{i}}{\sqrt{2D_{11}}} \\ \frac{1}{\sqrt{2D_{22}}} & \frac{1}{\sqrt{2D_{22}}} \end{bmatrix}, \quad \boldsymbol{\varphi} = \begin{Bmatrix} Q(x) \\ P(x) \end{Bmatrix}. \tag{24}$$

Substituting Eqs. (23), (24) into (22) yields

$$\begin{Bmatrix} K_{II} \\ -K_I \end{Bmatrix} = \lim_{x\to a} \sqrt{2\pi} \begin{bmatrix} \mathrm{Re}\{H(x)\} & \sqrt{\frac{D_{22}}{D_{11}}}\mathrm{Im}\{H(x)\} \\ -\sqrt{\frac{D_{11}}{D_{22}}}\mathrm{Im}\{H(x)\} & \mathrm{Re}\{H(x)\} \end{bmatrix} \begin{Bmatrix} Q(x) \\ P(x) \end{Bmatrix}, \tag{25}$$

where

$$H(x) = (a-x)^{\frac{1}{2}+\mathrm{i}\varepsilon} l^{-\mathrm{i}\varepsilon}. \tag{26}$$

Using Eq. (21), the stress intensity factors can be explicitly expressed as

$$K_I = \frac{-a^{3/2}}{\sqrt{\pi}RD_{22}(1-\eta^2)} \mathrm{Re}\left\{ 2^{\mathrm{i}\varepsilon} \left(\frac{a}{l}\right)^{\mathrm{i}\varepsilon} \int_{-1}^{1} \frac{\xi(1+\xi)^{\bar{r}}(1-\xi)^{r}}{\xi-1} \mathrm{d}\xi \right\} + \frac{\sqrt{\pi}}{\sqrt{a}} \times \sqrt{\frac{D_{11}}{D_{22}}} \mathrm{Im}\left\{ \frac{2^{\mathrm{i}\varepsilon}}{\int_{-1}^{1}(1+\xi)^{-\bar{r}}(1-\xi)^{-r}\mathrm{d}\xi} \left(\frac{a}{l}\right)^{\mathrm{i}\varepsilon} \left(F\sin\phi + \mathrm{i}F\cos\phi\sqrt{\frac{D_{22}}{D_{11}}} \right) \right\} \tag{27}$$

and

$$K_{II} = \frac{a^{3/2}}{\sqrt{\pi}R\sqrt{D_{11}D_{22}}(1-\eta^2)} \mathrm{Im}\left\{ 2^{\mathrm{i}\varepsilon} \left(\frac{a}{l}\right)^{\mathrm{i}\varepsilon} \int_{-1}^{1} \frac{\xi(1+\xi)^{\bar{r}}(1-\xi)^{r}}{\xi-1} \mathrm{d}\xi \right\} + \frac{\sqrt{\pi}}{\sqrt{a}} \mathrm{Re}\left\{ \frac{2^{\mathrm{i}\varepsilon}}{\int_{-1}^{1}(1+\xi)^{-\bar{r}}(1-\xi)^{-r}\mathrm{d}\xi} \left(\frac{a}{l}\right)^{\mathrm{i}\varepsilon} \left(F\sin\phi + \mathrm{i}F\cos\phi\sqrt{\frac{D_{22}}{D_{11}}} \right) \right\}. \tag{28}$$

Substituting the stress intensity factors in Eqs. (27) and (28) into the energy release rate

$$G = \frac{1}{4\cosh^2\pi\varepsilon} \left(D_{22}K_I^2 + D_{11}K_{II}^2 \right), \tag{29}$$

then, using the Griffith energy balance criterion at the contact edges

$$G = \Delta\gamma, \tag{30}$$

where $\Delta\gamma$ is the work of adhesion, leads to the following governing equation

$$\frac{F^2\pi D_{11}}{a} \frac{\left(\sin^2\phi + \frac{D_{22}}{D_{11}}\cos^2\phi\right)}{\left|\int_{-1}^{1}(1+\xi)^{-\bar{r}}(1-\xi)^{-r}\mathrm{d}\xi\right|^2} - \frac{2aF}{R(1-\eta^2)} \times \sqrt{\frac{D_{11}}{D_{22}}} \mathrm{Im}\left\{ \frac{\int_{-1}^{1} \frac{\xi(1+\xi)^{r}(1-\xi)^{\bar{r}}}{\xi-1}\mathrm{d}\xi}{\int_{-1}^{1}(1+\xi)^{-\bar{r}}(1-\xi)^{-r}\mathrm{d}\xi} \left(\sin\phi + \mathrm{i}\sqrt{\frac{D_{22}}{D_{11}}}\cos\phi \right) \right\} + \frac{a^3}{\pi R^2 D_{22}(1-\eta^2)^2} \left| \int_{-1}^{1} \frac{\xi(1+\xi)^{\bar{r}}(1-\xi)^{r}}{\xi-1}\mathrm{d}\xi \right|^2 - 4\Delta\gamma\cosh^2\pi\varepsilon = 0 \tag{31}$$

which describes the contact size a as a function of the pulling force F and the pulling angle ϕ.

For a special case, i.e., $\phi = 0$, which corresponds to the direction of the pulling force normal to the contact interface, the relation between the contact size a and the pulling force F can be simplified as

$$\frac{F^2\pi D_{22}}{a}\frac{1}{\left|\int_{-1}^{1}(1+\xi)^{-\bar{r}}(1-\xi)^{-r}\mathrm{d}\xi\right|^2}-\frac{2aF}{R(1-\eta^2)}\mathrm{Re}\left\{\frac{\int_{-1}^{1}\frac{\xi(1+\xi)^{r}(1-\xi)^{\bar{r}}}{\xi-1}\mathrm{d}\xi}{\int_{-1}^{1}(1+\xi)^{-\bar{r}}(1-\xi)^{-r}\mathrm{d}\xi}\right\}$$
$$+\frac{a^3}{\pi R^2 D_{22}(1-\eta^2)^2}\left|\int_{-1}^{1}\frac{\xi(1+\xi)^{\bar{r}}(1-\xi)^{r}}{\xi-1}\mathrm{d}\xi\right|^2-4\Delta\gamma\cosh^2\pi\varepsilon=0. \tag{32}$$

4. Analysis and discussion

4.1. The effects of mismatch parameter η

From Eq. (31), one can find that the relation between the pulling force F and the contact width $2a$ is affected by the elastic mismatch parameter η, which leads to an oscillatory singularity and a very complex expression. Motivated by recent studies (Chen and Gao, 2006a,b,c; Chen and Gao, 2007; Chen and Wang, 2006), where the Dundurs' parameter β has a minor effect on the pull-off process when the pulling force is normal to the contact interface.

It can be shown in the present model that the normalized pulling force $F/\Delta\gamma$ depends on the normalized contact half-width a/R via four parameters, D_{11}/D_{22}, $\Delta\gamma D_{22}/R$, η and ϕ. For the case with a fixed pulling angle $\phi \neq 0$, numerical calculation find that η has a significant effect on the pull-off process and the difference between the non-oscillatory ($\eta = 0$) and oscillatory solutions ($\eta \neq 0$) increases with an increasing value of η.

For a special case, $\phi = 0$, i.e., the pulling force normal to the contact interface, the relation between the pulling force and the contact half-width is expressed by Eq. (32), where we find that the normalized pulling force $F/\Delta\gamma$ depends on the normalized contact half-width a/R via three parameters, $\Delta\gamma D_{22}/R$, η and ϕ, except for the non-dimensional parameter D_{11}/D_{22}. For a fixed value of $\Delta\gamma D_{22}/R$, the difference between the non-oscillatory and oscillatory solutions with different values of η is very small when $\eta \leqslant 0.25$. Especially, the critical pull-off force and pull-off contact half-width are hardly influenced by a wide range of η, so that the non-oscillatory solution can be a very good approximation to the oscillatory cases. Fig. 2 is shown as an example.

Furthermore, one can easily infer from the conclusions of Fig. 2 that the non-oscillatory solution is also adaptive to the model of a rigid or an elastic isotropic cylinder in contact with an isotropic or a transversely isotropic substrate only if the direction of pulling is normal to the contact interface. This inference is consistent well with the former studies about adhesive contacts (Chen and Gao, 2006a,b,c; Chen and Gao, 2007; Chen

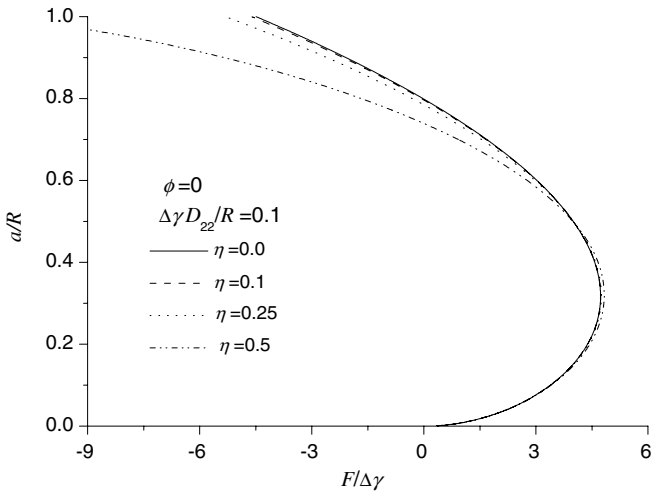

Fig. 2. Normalized pulling force $F/\Delta\gamma$ as a function of normalized contact half-width a/R for $\Delta\gamma D_{22}/R = 0.1$ and different values of $\eta = 0.0, 0.1, 0.25, 0.5$.

and Wang, 2006), which has also been used in the classical contact problems (for examples, Hertz, 1882; Johnson, 1985).

An interesting issue is to study the critical pull-off force, pull-off contact width as well as the adhesion strength, which can be obtained from numerical calculation if $\phi \neq 0$. Examples are shown in Figs. 3–5. In each figure, we take $\eta = 0.1$, four different values of D_{11}/D_{22} and two values of $\Delta\gamma D_{22}/R$. The results for isotropic case, i.e., $D_{11}/D_{22} = 1.0$, are also shown in the figures. Fig. 3 shows the normalized critical pull-off force $F^{\mathrm{p}}/F_0^{\mathrm{p}}$ as a function of the pulling angle ϕ, where the subscript "0" denotes $\phi = 0$ and the superscript "p" denotes pull-off. From Fig. 3, one can see that the normalized critical pull-off force does not depend on the non-dimensional parameter $\Delta\gamma D_{22}/R$ but depends strongly on the non-dimensional value of D_{11}/D_{22} and pulling angle ϕ. As the value of D_{11}/D_{22} increases, the normalized pull-off force varies stronger and stronger with the direction of pulling. The normalized pull-off force attains the maximum value always at $\phi = 0$ when the elastic anisotropy becomes stronger. Especially, for the case of $D_{11}/D_{22} \geqslant 1000$, the maximum pull-off force is almost an order of magnitude larger than the minimum one.

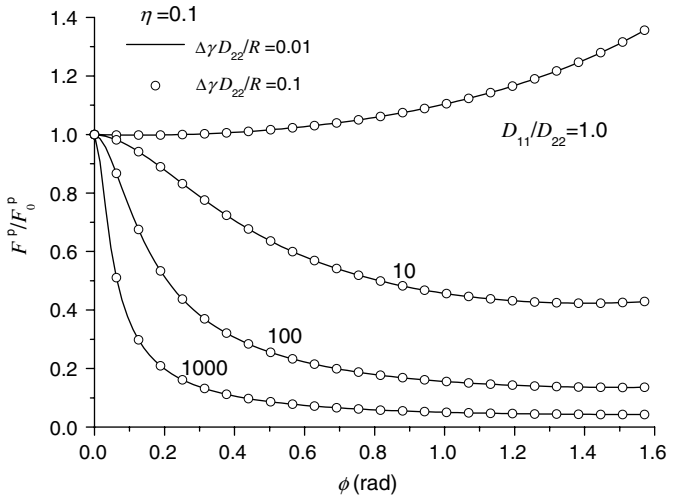

Fig. 3. Plots of the normalized pull-off force $F^{\mathrm{p}}/F_0^{\mathrm{p}}$ as a function of different pulling angle ϕ for $\eta = 0.1$, $\Delta\gamma D_{22}/R = 0.1$, 0.01 and different values of D_{11}/D_{22}, in which F_0^{p} denotes the pull-off force with $\phi = 0$.

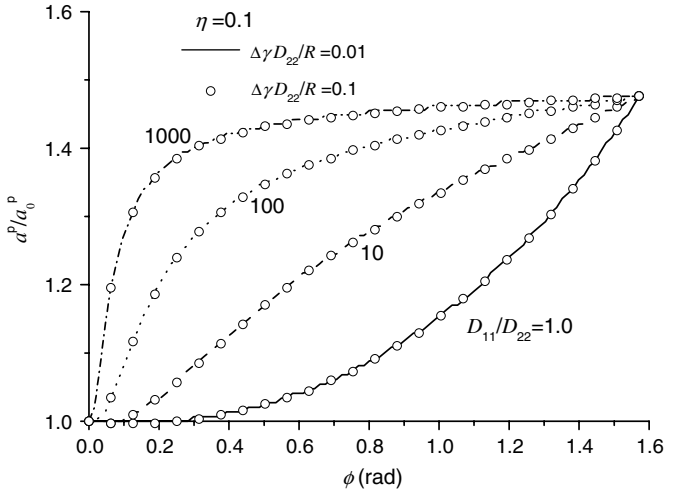

Fig. 4. Plots of the normalized pull-off contact half-width $a^{\mathrm{p}}/a_0^{\mathrm{p}}$ as a function of different pulling angles ϕ for $\eta = 0.1$, $\Delta\gamma D_{22}/R = 0.1$, 0.01 and different values of D_{11}/D_{22}, in which a_0^{p} denotes the pull-off contact half-width with $\phi = 0$.

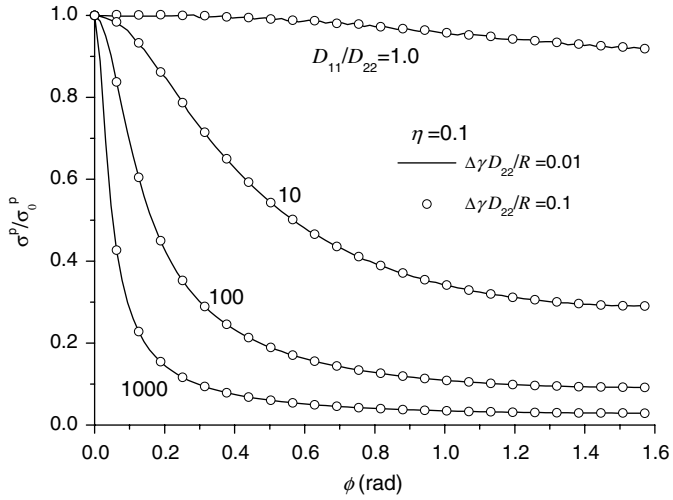

Fig. 5. Plots of the normalized adhesion strength σ^p/σ_0^p as a function of different pulling angles ϕ for $\eta = 0.1$, $\Delta\gamma D_{22}/R = 0.1$, 0.01 and different values of D_{11}/D_{22}, in which σ_0^p denotes the adhesion strength with $\phi = 0$.

Fig. 4 shows the normalized pull-off contact width as a function of pulling angle ϕ with the same parameters used in Fig. 3. From Fig. 4, one can see that the normalized pull-off contact width also does not depend on the non-dimensional parameter $\Delta\gamma D_{22}/R$ but senses the value of D_{11}/D_{22} strongly. The maximum pull-off contact width always emerges at $\phi = \pi/2$. An interesting phenomenon can be found from Figs. 3 and 4. The pull-off force and pull-off contact half-width for $D_{11}/D_{22} = 1.0$ in Figs. 3 and 4, respectively, increase when the pulling angle ϕ increases, which means that the friction force is proportional to the contact area in the isotropic case and is consistent with the experiment results (Carpick et al., 1996, 2004; Enachescu et al., 1999). However, in the transversely isotropic case, i.e., $D_{11}/D_{22} \neq 1.0$, the pull-off force decreases while the pull-off contact half-width increases for a determined value of D_{11}/D_{22}, which should be verified by the corresponding experiment in future.

The adhesion strength σ^p is defined as the ratio of the pull-off force to pull-off contact width. Normalized adhesion strength σ^p/σ_0^p as a function of the pulling angle ϕ is shown in Fig. 5 with the same parameters used in Figs. 3 and 4. It shows that D_{11}/D_{22}, i.e., the elastic anisotropy, has significant effects on the normalized adhesion strength σ^p/σ_0^p. As the value of D_{11}/D_{22} increases, the normalized adhesion strength σ^p/σ_0^p varies strongly with the direction of the pulling force. Furthermore, when the value of D_{11}/D_{22} is larger than 1000, the maximum adhesion strength, which emerges at $\phi = 0$, can be an order of magnitude larger than the minimum one attained at $\phi = \pi/2$ and the value of adhesion strength decreases quickly when the angle deviates $\phi = 0$.

From above, one can see that a switch between attachment and detachment can thus be accomplished just by shifting the pulling angle. For practical application, it is helpful for designing synthetic adhesion systems in engineering using piezoelectric materials (e.g., PZT-4, barium titanate) or fiber-reinforced composites where all fibers are in parallel.

4.2. The non-oscillatory solution for the case of $\phi = 0$

For the case of $\phi = 0$, we have found from above that the non-oscillatory solution can be a good approximation to oscillatory one for the bimaterial adhesive contact model. Explicit expressions of the pull-off force, pull-off contact width and the adhesion strength in the non-oscillatory solution will be given, which is very convenient to be used for engineering.

The non-oscillatory condition corresponds that

$$\eta = 0 \tag{33}$$

which yields

$$\varepsilon = 0, \quad r = \frac{1}{2}. \tag{34}$$

Substituting the condition of $\phi = 0$ and Eqs. (33) and (34) into Eq. (21) yields

$$Q(x) = 0 \tag{35}$$

and

$$P(x) = \frac{\frac{a^2}{2} - x^2}{RD_{22}\sqrt{a^2 - x^2}} - \frac{F}{\pi\sqrt{a^2 - x^2}}. \tag{36}$$

Then the stress intensity factor can be obtained

$$K_I = \frac{\sqrt{\pi}a^{3/2}}{2RD_{22}} + \frac{F}{\sqrt{\pi a}}. \tag{37}$$

Substituting the stress intensity factor in Eq. (37) into the following Griffith energy balance criterion,

$$G = \frac{D_{22}K_I^2}{4} = \Delta\gamma \tag{38}$$

yields the external loading F as a function of the contact half-width a

$$F = \frac{-\pi a^2}{2RD_{22}} + 2\sqrt{\frac{\pi a \Delta\gamma}{D_{22}}}. \tag{39}$$

Using the following equation

$$\frac{\partial F}{\partial a} = 0 \tag{40}$$

yields the pull-off contact half-width as

$$a_0^{\mathrm{p}} = \left(\frac{R^2 D_{22}\Delta\gamma}{\pi}\right)^{\frac{1}{3}} \tag{41}$$

and the pull-off force

$$F_0^{\mathrm{p}} = \frac{3}{2}\left(\frac{\pi R \Delta\gamma^2}{D_{22}}\right)^{\frac{1}{3}}, \tag{42}$$

where the subscript "0" denotes the case of $\phi = 0$.

The adhesion strength σ_{p} can be obtained from Eqs. (31) and (42) as,

$$\sigma_0^{\mathrm{p}} = \frac{F_0^{\mathrm{p}}}{2a_0^{\mathrm{p}}} = \frac{3}{4}\left(\frac{\pi^2\Delta\gamma}{D_{22}^2 R}\right)^{1/3}. \tag{43}$$

Eqs. (39)–(43) can be a good approximation to the adhesive contact model of two transversely isotropic materials with the direction of the pulling force normal to the contact interface.

4.3. Special case – isotropic bimaterial case

If the transversely isotropic materials degenerate to isotropic materials, i.e.,

$$D_{11} = D_{22} = \frac{2(1 - \nu_1^2)}{E_1} + \frac{2(1 - \nu_2^2)}{E_2} = \frac{2}{E^*}, \tag{44}$$

$$W_{21} = -W_{12} = \frac{(1 - 2\nu_1)(1 + \nu_1)}{E_1} - \frac{(1 - 2\nu_2)(1 + \nu_2)}{E_2}, \tag{45}$$

where E_1 and v_1 denote the Young's modulus and Poisson ratio of the upper cylinder, E_2 and v_2 are those of the lower substrate.

Then, the oscillatory solution will be identical to that in Chen and Gao (2006a) and the non-oscillatory solution will be the same as the classical two-dimensional JKR theory (Barquins, 1988; Chaudhury et al., 1996; Chen and Gao, 2006a).

For the cases of adhesive contact between a rigid cylinder and a transversely isotropic material or an isotropic elastic cylinder and a transversely isotropic material, the solutions can be obtained very easily from above.

Acknowledgments

The work reported here is supported by NSFC (Nos. 10672165 and 10732050) and KJCX2-YW-M04SC.

References

Arnold, J.W., 1974. Adaptive features on the tarsi of cockroaches (Insecta: Dictyoptera). Int. J. Insect Morphol. Embryol. 3, 317–334.

Arzt, E., Gorb, S., Spolenak, R., 2003. From micro to nano contacts in biological attachment devices. Proc. Natl. Acad. Sci. USA 100, 10603–10606.

Autumn, K., Liang, Y.C., Hsieh, S.T., Zesch, W., Chan, W.P., Kenny, T.W., Fearing, R., Full, R.J., 2000. Adhesion forces of a single gecko foot–hair. Nature 405, 681–685.

Baney, J.M., Hui, C.Y., 1997. A cohesive zone model for the adhesion of cylinders. J. Adhes. Sci. Technol. 11, 393–406.

Barquins, M., 1988. Adherence and rolling kinetics of a rigid cylinder in contact with a natural rubber surface. J. Adhes. 26, 1–12.

Barthel, E., 1998. On the description of the adhesive contact of spheres with arbitrary interaction potentials. J. Colloid Interface Sci. 200, 7–18.

Carpick, R.W., Agrait, N., Ogletree, D.F., Salmeron, M., 1996. Variation of the interfacial shear strength and adhesion of a nanometer sized contact. Langmuir 12, 3334–3340.

Carpick, R.W., Flater, E.E., Sridharan, K., Ogletree, D.F., Salmeron, M., 2004. Atomic-scale friction and its connection to fracture mechanics. JOM 56, 48–52.

Carrier, G.F., Krook, M., Pearson, C.E., 1983. Functions of a Complex Variable. Hod brooks, Ithaca, New York.

Chaudhury, M.K., Weaver, T., Hui, C.Y., Kramer, E.J., 1996. Adhesion contact of cylindrical lens and a flat sheet. J. Appl. Phys. 80, 30–37.

Chen, S., Gao, H., 2006a. Non-slipping adhesive contact of an elastic cylinder on stretched substrates. Proc. R. Soc. Lond. A 462, 211–228.

Chen, S., Gao, H., 2006b. Generalized Maugis–Dugdale model of an elastic cylinder in non-slipping adhesive contact with a stretched substrate. Int. J. Mater. Res. 97, 584–593.

Chen, S., Gao, H., 2006c. Non-slipping adhesive contact between mismatched elastic spheres: a model of adhesion mediated deformation sensor. J. Mech. Phys. Solids 54, 1548–1567.

Chen, S., Gao, H., 2007. Non-slipping adhesive contact between mismatched elastic cylinders. Int. J. Solids Struct. 44, 1939–1948.

Chen, S., Gao, H., 2007. Bio-inspired mechanics of reversible adhesion: orientation-dependent adhesion strength for non-slipping adhesive contact with transversely isotropic elastic materials. J. Mech. Phys. Solids 55, 1001–1015.

Chen, S., Wang, T., 2006. General solution to two-dimensional non-slipping JKR model with a pulling force in an arbitrary direction. J. Colloid Interface Sci. 302, 363–369.

Chu, Y.S., Dufour, S., Thiery, J.P., Perez, E., Pincet, F., 2005. Johnson–Kendall–Roberts theory applied to living cells. Phys. Rev. Lett. 94 (2), 028102.

Derjaguin, B.V., Muller, V.M., Toporov, Y.P., 1975. Effect of contact deformations on the adhesion of particles. J. Colloid Interface Sci. 53, 314–326.

Dongye, C., Ting, T.C.T., 1989. Explicit expression of Barnett–Lothe tensors and their associated tensors for orthotropic materials. Q. Appl. Math. 47, 723–734.

Dugdale, D.S., 1960. Yielding of steel sheets containing slits. J. Mech. Phys. Solids 8, 100–104.

Enachescu, M., van den Oetelarr, R.J.A., Carpick, R.W., Ogletree, D.F., Flipse, C.F.J., Salmeron, M., 1999. Observation of proportionality between friction and contact area at the nanometer scale. Tribol. Lett. 7, 73–78.

Gao, H., Yao, H., 2004. Shape insensitive optimal adhesion of nanoscale fibrillar structures. Proc. Natl. Acad. Sci. USA 101, 7851–7856.

Gao, H., Wang, X., Yao, H., Gorb, S., Arzt, E., 2005. Mechanics of hierarchical adhesion structures of gecko. Mech. Mater. 37, 275–285.

Geim, A.K., Dubonos, S.V., Grigorieva, I.V., Novoselov, K.S., Zhukov, A.A., Shapoval, S., 2003. Microfabricated adhesive mimicking gecko foot–hair. Nat. Mater. 2, 461–463.

Glassmaker, N.J., Jagota, A., Hui, C.Y., Kim, J., 2004. Design of biomimetic fibrillar interface: 1. Making contact. J. R. Soc. Interface 1, 23–33.

Greenwood, J.A., 1997. Adhesion of elastic spheres. Proc. R. Soc. Lond. A 453, 1277–1297.

Greenwood, J.A., Johnson, K.L., 1998. An alterative to the Maugis model of adhesion between elastic spheres. J. Phys. D: Appl. Phys. 31, 3279–3290.
Hertz, H., 1882. On the contact of elastic solids. J. Reine Angew. Math. 92, 156–171.
Hui, C.Y., Glassmaker, N.J., Tang, T., Jagota, A., 2004. Design of biomimetic fibrillar interface: 2. Mechanics of enhanced adhesion. J. R. Soc. Interface 1, 35–48.
Hurtado, J.A., Kim, K.S., 1999. Scale effects in friction of single-asperity contacts. I. From concurrent slip to single-dislocation-assisted slip. Proc. R. Soc. Lond. A 455, 3363–3384.
Hwu, C., 1993. Fracture parameters for the orthotropic bimaterial interface cracks. Eng. Fract. Mech. 45, 89–97.
Johnson, K.L., 1985. Contact Mechanics. Cambridge University Press, New York.
Johnson, K.L., Greenwood, J.A., 1997. An adhesion map for the contact of elastic spheres. J. Colloid Interface Sci. 192, 326–333.
Johnson, K.L., Kendall, K., Roberts, A.D., 1971. Surface energy and the contact of elastic solids. Proc. R. Soc. Lond. A 324, 301–313.
Kendall, K., 1975. The effects of shrinkage on interfacial cracking in a bonded laminate. J. Phys. D: Appl. Phys. 8, 1722–1732.
Kim, K.S., McMeeking, R.M., Johnson, K.L., 1998. Adhesion, slip cohesive zone and energy fluxes for elastic spheres in contact. J. Mech. Phys. Solids 46, 243–266.
Maugis, D., 1992. Adhesion of spheres: The JKR-DMT transition using a Dugdale model. J. Colloid Interface Sci. 150, 243–269.
Morrow, C., Lovell, M., Ning, X., 2003. A JKR-DMT transition solution for adhesive rough surface contact. J. Phys. D: Appl. Phys. 36, 534–540.
Persson, B.N.J., 2003. On the mechanism of adhesion in biological systems. J. Chem. Phys. 118 (16), 7614–7621.
Robbe-Valloire, F., Barquins, M., 1998. Adhesive contact and kinetics of adherence between a rigid cylinder and an elastomeric solid. Int. J. Adhes. Adhes. 18, 29–34.
Roth, L.M., Willis, E.R., 1952. Tarsal structure and climbing ability of cockroaches. J. Exp. Biol. 119, 483–517.
Savkoor, A.R., Briggs, G.A.D., 1977. The effect of a tangential force on the contact of elastic solids in adhesion. Proc. R. Soc. Lond. A356, 103–114.
Schwarz, U.D., 2003. A generalized analytical model for the elastic deformation of an adhesive contact between a sphere and a flat surface. J. Colloid Interface Sci. 261, 99–106.
Slifer, E.H., 1950. Vulnerable areas on the surface of the tarsus and pretarsus of the grasshopper (Acrididae, Orthoptera) with special reference to the arolium. Ann. Entomol. Soc. Am. 43, 173–188.
Ting, T.C.T., 1996. Anisotropic Elasticity. Oxford University Press, New York.
Wu, K.C., 1990. Stress intensity factors and energy release rate for interfacial cracks between dissimilar anisotropic materials. J. Appl. Mech. 57, 882–886.
Yao, H., Gao, H., 2006. Mechanics of robust and releasable adhesion in biology: bottom-up designed hierarchical structures of gecko. J. Mech. Phys. Solids 54, 1120–1146.